JOURNAL OF GEOPHYSICAL RESEARCH: SPACE PHYSICS, VOL. 118, 5967–5978, doi:10.1002/jgra.50567, 2013

Earth's collision with a solar filament on 21 January 2005: Overview

J. U. Kozyra,[1] W. B. Manchester IV,[1] C. P. Escoubet,[2] S. T. Lepri,[1] M. W. Liemohn,[1] W. D. Gonzalez,[3] M. W. Thomsen,[4] and B. T. Tsurutani[5]

Received 25 January 2013; revised 29 August 2013; accepted 11 September 2013; published 1 October 2013.

[1] On 21 January 2005, one of the fastest interplanetary coronal mass ejections (ICME) of solar cycle 23, containing exceptionally dense plasma directly behind the sheath, hit the magnetosphere. We show from charge-state analysis that this material was a piece of the erupting solar filament and further, based on comparisons to the simulation of a fast CME, that the unusual location of the filament material was a consequence of three processes. As the ICME decelerated, the momentum of the dense filament material caused it to push through the flux rope toward the nose. Diverging nonradial flows in front of the filament moved magnetic flux to the sides of the ICME. At the same time, reconnection between the leading edge of the ICME and the sheath magnetic fields worked to peel away the outer layers of the flux rope creating a remnant flux rope and a trailing region of newly opened magnetic field lines. These processes combined to move the filament material into direct contact with the ICME sheath region. Within 1 h after impact and under northward interplanetary magnetic field (IMF) conditions, a cold dense plasma sheet formed within the magnetosphere from the filament material. Dense plasma sheet material continued to move through the magnetosphere for more than 6 h as the filament passed by the Earth. Densities were high enough to produce strong diamagnetic stretching of the magnetotail despite the northward IMF conditions and low levels of magnetic activity. The disruptions from the filament collision are linked to an array of unusual features throughout the magnetosphere, ionosphere, and atmosphere. These results raise questions about whether rare collisions with solar filaments may, under the right conditions, be a factor in producing even more extreme events.

Citation: Kozyra, J. U., W. B. Manchester IV, C. P. Escoubet, S. T. Lepri, M. W. Liemohn, W. D. Gonzalez, M. W. Thomsen, and B. T. Tsurutani (2013), Earth's collision with a solar filament on 21 January 2005: Overview, *J. Geophys. Res. Space Physics*, *118*, 5967–5978, doi:10.1002/jgra.50567.

1. Introduction

[2] Solar filaments are coronal condensations of dense, chromospheric-temperature plasma that are supported by relatively strong magnetic fields of active regions or by weaker fields in the case of quiescent filaments (see review by *Rust* [1999]). This chromospheric material is 100 times denser than the coronal material and 100 times cooler. It also contains significantly more singly and low charge-state ions characteristic of these cooler temperatures [*Lepri and Zurbuchen*, 2010; *Gilbert et al*., 2012]. When active regions erupt, the filaments are caught up in the explosive release of plasma and magnetic fields that form a coronal mass ejection (CME).

[3] CMEs commonly have a three-part structure as they lift off the Sun [cf. *Illing and Hundhausen*, 1985]: (1) a bright outer loop formed of dense coronal material from the overlying helmet streamer [*Tsurutani and Gonzalez*, 1994], (2) a dark cavity which corresponds to the magnetic flux rope itself, and (3) a bright core believed to be associated with the erupting solar filament. After leaving the Sun, the disturbance is termed an ICME (I = interplanetary) rather than a CME, the distinction being that its structure is modified, sometimes significantly, during propagation through interplanetary space.

[4] Despite observations indicating that more than 70% of active region eruptions involve solar filaments [*Gopalswamy et al*., 2003], filaments are rarely identifiable in ICMEs at Earth [cf. *Forsyth et al*., 2006; *Wimmer-Schweingruber et al*., 2006; *Zurbuchen and Richardson*, 2006; *Crooker and Horbury*, 2006]. Only 4% of ICMEs measured in situ at 1 AU (11 out of 283 during 1998–2008) have been found to date to contain detectable amounts of low charge-state

[1]AOSS Department, University of Michigan, Ann Arbor, Michigan, USA.
[2]ESA/ESTEC, Noordwijk, Netherlands.
[3]National Institute of Space Research, Sao Jose Dos Campos, Brazil.
[4]Los Alamos National Laboratory, Los Alamos, New Mexico, USA.
[5]Jet Propulsion Laboratory, Pasadena, California, USA.

Corresponding author: J. U. Kozyra, AOSS Department, University of Michigan, 1414-A Space Research Bldg., 2455 Hayward St., Ann Arbor, MI 48109-2143, USA. (jukozyra@umich.edu)

2169-9380/13/10.1002/jgra.50567

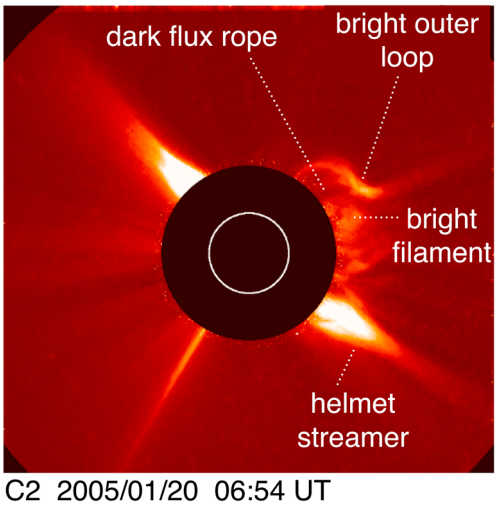

Figure 1. Image by the SOHO LASCO C2 coronagraph on 20 January 2005 after cosmic ray removal shows the characteristic three-part structure of a coronal mass ejection near the Sun. Also shown is a typical helmet streamer. Adapted from *Rodriguez et al*. [2008].

heavy ions characteristic of the cool material in solar filaments [*Lepri and Zurbuchen*, 2010]. The authors identified filamentary material using the presence of at least two elements (of the three C, O, and Fe) with simultaneous low charge states. They did not consider He^+, a key contribution of the present paper.

[5] The reasons for the disconnect between remote and in situ observations of solar filament material are a long-standing mystery in space physics. The small numbers of detectable solar filament events at 1 AU suggest that only under unusual circumstances does the filament material survive transit of the corona and transport to Earth with its high density and low charge-state signatures preserved. *Gruesbeck et al*. [2012] modeled the ionization of cool dense prominence material in an example CME eruption and found that the dense material was able to escape with low levels of ionization beyond the freeze-in point, assuming typical expansion speeds and very high densities $\sim 10^{10}$ cm^{-3}.

[6] The position of the filament material with respect to the magnetic field structure of the ICME is an important factor in its geo-effectiveness. For example, whether northward or southward interplanetary magnetic field (IMF) accompanies the filament material determines how the material enters the magnetosphere and the characteristics of the plasma sheet that develops. There is no consistent spatial ordering of the cold filament material within an ICME by the time it reaches the Earth despite the characteristic three-part structure of the outgoing CME at the Sun [*Illing and Hundhausen*, 1985]. *Lepri and Zurbuchen* [2010] found that in only 45% of cases in which a filament was identified, did it appear in the trailing third of the ICME, as one would expect. In 35% of the cases, the filament material actually appeared in the leading third of the ICME (as was the case for the 21 January 2005 event studied here) and in the remaining 20% of cases, it appeared in the middle third of the ICME. Filament material has even been identified outside the trailing edge of an ICME [*Lepri and Zurbuchen*, 2010], and in the sheath region in front of the magnetic cloud structure (in this paper). All the significant filaments identified to date have been different in their charge-state composition and in the distribution of cold filament material within and surrounding the ICME [cf. *Burlaga et al*., 1998; *Skoug et al*., 1999; *Farrugia et al*., 2002; *Lepri and Zurbuchen*, 2010; *Sharma et al*., 2013] suggesting that complex processes are responsible for their transport to 1 AU.

[7] Observations on 21 January 2005 show unusual geospace consequences tied directly to a significant solar filament impact. Although this type of impact may be relatively rare, it is of intense interest. We now know that high-density plasma can amplify the damaging effects of magnetic storms [cf. *Lyons*, 2000; *Zhou and Tsurutani*, 2003; *Liou et al*., 2007; *Laundal and Østgaard*, 2008; *Weigel*, 2010]. The highest solar wind densities in ICMEs are found in solar filament material [*Crooker et al*., 2000] and ICMEs are responsible for the most severe types of space weather [cf. *Tsurutani et al*., 1988; *Richardson et al*., 2001]. For example, the March 2001 CME [*Farrugia et al*., 2006] had densities just after the shock in excess of 100 cm^{-3}, which is thought to have enhanced its geo-effectiveness. The magnetic storm that resulted reached min $Dst < -250$ nT.

[8] In this first report we summarize new information about the transport of a solar filament to Earth and key features of its interaction with geospace. A more detailed treatment of the conditions that enabled the solar filament to reach Earth and of the resulting unusual features that it generated in the magnetosphere, ionosphere, and atmosphere will be provided in later publications.

2. What Happened at the Sun?

[9] At ~17:11 UT on 21 January 2005, one of the fastest ICMEs of solar cycle 23 hit the Earth. The probable solar source of this disturbance identified by *Foullon et al*. [2007, hereafter referred to as F2007] and *Rodriguez et al*. [2008, hereafter referred to as R2008] was a halo CME (shown in Figure 1) associated with an X7.1 flare from NOAA active region 10720. The halo CME reached the LASCO C2 field of view at 06:54 UT. However, a strong solar particle event rendered all subsequent images of this CME unusable in both LASCO C2 and C3. An estimation of its speed based on observations of Type II burst-associated shock waves in the solar wind and corona and in situ measurements of these same shock waves and related structures at 1 AU indicate the ICME may have reached 3000 km/s between 3 and 50 solar radii before decelerating down to 1000 km/s upstream of Earth at 1 AU [*Pohjolainen et al*., 2007]. The speed of the ICME is consistent with an arrival time late on 21 January. The ICME travel time to Earth was just 34 h [*Pohjolainen et al*., 2007; *Foullon et al*., 2007].

[10] F2007 analyzed the ICME in great detail with observations from Cluster, ACE, Wind, and Geotail at 1 AU. They identified a magnetic cloud with onset at 00:40 UT on 22 January, nearly 7 h after the shock arrived, based largely on plasma beta values < 0.2. The rotation of the field in the magnetic cloud (MC) was not pronounced and no model was able to provide a successful fit to the magnetic field data. F2007 concluded that the Earth encountered the flanks of a MC in strong expansion with axis nearly perpendicular to the ecliptic. In this scenario, the spacecraft observed the

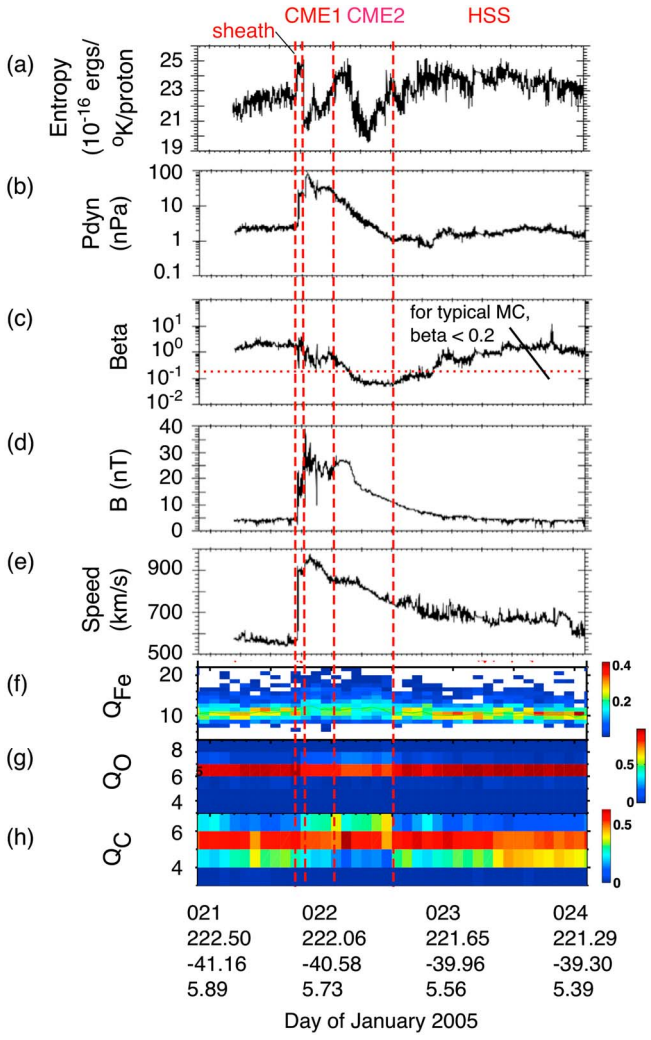

Figure 2. Solar wind parameters from the ACE spacecraft over the interval 21–24 January 2005 show evidence for two interacting CMEs. Included at a 1 min resolution are (a) entropy, (b) dynamic pressure, (c) plasma beta, (d) magnetic field strength, and (e) solar wind speed propagated to the bow shock normal in the OMNIWeb database. Over the interval 00:40 UT – 08:41 UT on 22 January, level 2 solar wind parameters were not available due to contamination by a strong solar particle event. Missing observations were filled in using search mode data that has an ~33 minute time resolution (courtesy of R. Skoug and H. Elliott, 2005) and propagated to 10 R_E using the observed solar wind velocity, V_x. (f–h) Charge-state composition at a 2 h time resolution is shown. Because of the coarse resolution, it was not necessary to add a time delay to 1 AU.

MC at large impact parameter and therefore did not sample the typical rotation of the magnetic field at its core. Hence, the structure was identified as magnetic cloud-like (MCL). R2008 suggested an alternative scenario in which the axis of the MCL had a horizontal orientation in the ecliptic plane with the satellites sampling the leg at small impact parameter. Both scenarios are completely consistent with the magnetic field observations at 1 AU.

[11] Between the shock and the MCL, F2007 identified a noncompressive density enhancement (NCDE) produced by an enrichment in helium. A magnetic arcade of field lines associated with the NCDE was still attached to the Sun. Plasma beta values in this interval were outside the probable range for a magnetic cloud. In the present work, we identify the NCDE as a solar filament based on the presence of He^+ and the magnetic arcade as a remnant magnetic cloud based on comparison to a simulation of a fast ICME. When we identify the magnetic field structure behind the shock as a CME, we are in effect proposing a CME-CME interaction, since there is clear evidence for a second CME at the location identified by F2007. R2008 discussed the very good possibility that the ICME on 21–22 January was actually composed of two interacting halo CMEs. The authors identified as a second candidate an earlier full halo CME associated with an X1.3 class flare which lifted off at ~08:29 UT on 19 January at estimated speeds of 1844–2020 km/s. However, the timing of the arrival at Earth late on 21 January is inconsistent with a CME traveling at those high speeds. There are indications that this halo CME actually reached Earth on 20 January at ~15:00 UT with a travel time of ~30.5 h.

[12] We investigate further the evidence for interacting CMEs. Figure 2 displays solar wind parameters from 13 UT on 21 January to 02 UT on 24 January observed by the Advanced Composition Explorer (ACE) spacecraft [*Gloeckler et al.*, 1998; *Stone et al.*, 1998] upstream of the Earth. Parameters in Figures 2b–2e, taken at a 1 min cadence, were propagated to the time of bow shock encounter in the OMNIWeb database at http://omniweb.gsfc.nasa.gov. However, in this figure (and Figure 3), level 2 solar wind parameters were not available in the interval 00:40 UT to 08:41 UT on 22 January, due to contamination of the observations by a strong solar particle event. ACE observations were supplemented in this interval with search mode data that has an ~33 min time resolution (courtesy of R. Skoug and H. Elliott, 2005). These reprocessed data were propagated from ACE to 10 R_E using the observed solar wind velocity (V_x). Figures 2f–2h give the charge-state distributions for Fe, O, and C at a 2 h cadence measured by the Solar Wind Ion Composition Spectrometer (SWICS) on ACE. Due to the coarser time resolution of these data, it was not necessary to propagate these to bow shock encounter. The same is true for the He^+/He^{2+} ratio in Figure 3g.

[13] Figure 2a displays the entropy per proton defined as $S = k \ln (T_p^{1.5}/N_p)$ calculated from ACE observations where S is in erg/K/proton, $k = 1.38 \times 10^{-16}$ erg/K, T_p is in °K, and N_p is in cm^{-3} [*Burlaga et al.*, 1990]. Entropy is used to identify plasmas of different origins. Based on low entropy values, we identify two CMEs in the figure and mark their start and end times with vertical red dashed lines. A coronal hole (CH140) was in Earth-facing position during 18–20 January with the effects of the associated high-speed stream seen at Earth on 22–24 January (from the Coronal Hole History at http://www.solen.info/solar/coronal_holes.html). The exact onset time of the high-speed stream at Earth was not discernable due to its interaction with the preceding ICME activity but it dominated solar wind conditions later in the day on 22 January. The interaction between the high-speed stream and CME2 may have also complicated the identification of its trailing edge.

[14] In CME2 (identified by F2007), plasma beta dipped to values <0.2 (Figure 2c), which is typical of CMEs [cf. *Lepping et al.*, 2003]. On this basis, F2007 placed the start

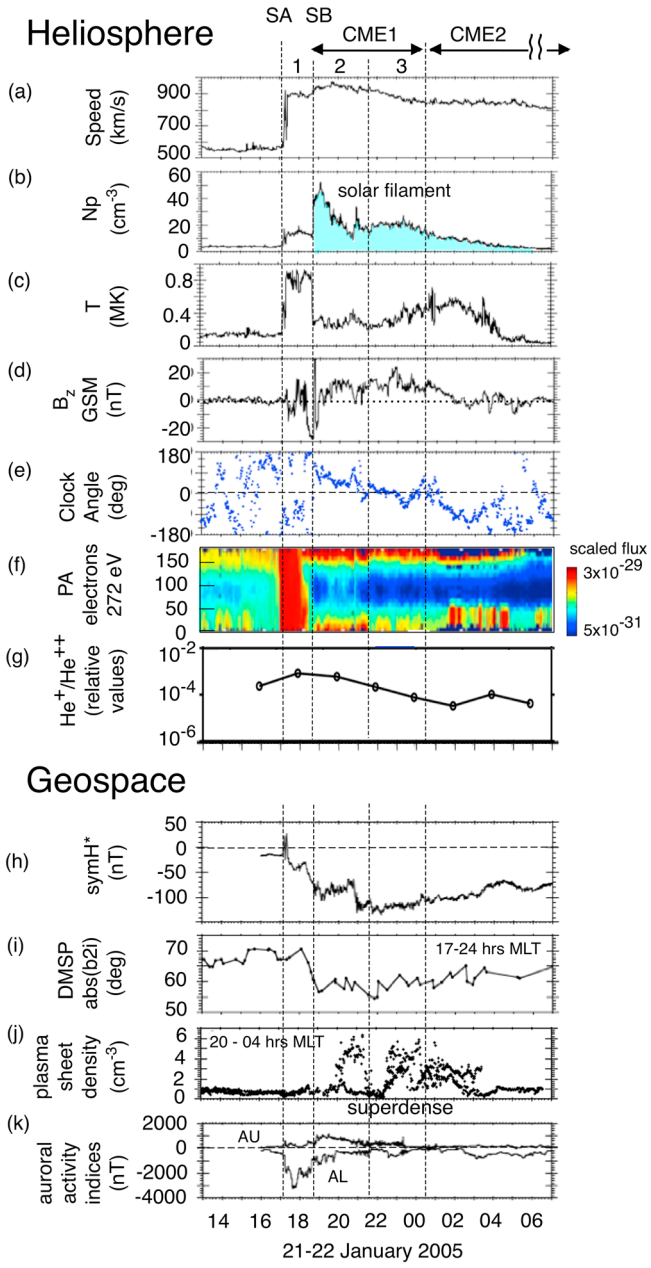

Figure 3. An expanded view is given of solar wind and geospace conditions during CME1, which contained significant solar filament material. Regions 1, 2, and 3 correspond to the sheath, remnant flux rope, and opened outer portion of the original flux rope. These three regions are depicted schematically in Figure 4. See text for more details.

of CME2 at 00:40 UT and its end at 21:20 UT on 22 January. At the trailing edge of CME2, beta recovered to values >0.2 and dynamic pressure returned to low values typical of high-speed streams (Figure 2b). A dip in plasma beta also accompanied CME1 but beta exceeded typical values used to identify CMEs. The higher beta could be due to the presence of the dense solar filament material but may also be an effect of the CME-CME interaction process as seen for multiple MC events [*Wang et al*., 2003; *Lugaz et al*., 2005]. This later scenario is consistent with the shorter duration of CME1. Figures 2f, 2g, and 2h indicate an increase in high charge states of Fe, O, and C, respectively in association with both CME1 and CME2. Charge states were lower in the solar wind preceding the shock and in the high-speed stream following CME2. On the basis of this rather abrupt change in charge-state composition, the trailing edge of CME2 may have arrived as early as 12:00 UT on 22 January.

[15] We associate CME1 with the halo CME that lifted off the Sun and was seen by LASCO C2 on 20 January at 0654 UT. A probable solar source for CME2 is the C8-class solar flare in the same active region (10720) a little more than 9 h later peaking at 16:14 UT on 20 January. There is no way to verify whether a halo CME was associated with this flare activity because the LASCO coronagraph images were completely unusable due to contamination by the previously mentioned strong solar proton event. However, the travel time to Earth of 32.4 h is reasonable to account for the arrival of CME2 at 00:40 UT on 22 January.

[16] We now return to CME1 the focus of the present study. Figure 3 gives an expanded view of solar wind parameters over the shorter time interval associated with ICME1. There are two extremely unusual features. First, as we will demonstrate, ICME1 contained a large amount of solar filament material—only one of a few such cases ever reported [cf. *Burlaga et al*., 1998; *Skoug et al*., 1999; *Farrugia et al*., 2002]. Second, the filament material was displaced from its expected position in the ICME. It was directly behind the sheath, at the leading edge of the flux rope (illustrated in Figure 4), a configuration that does not fit the simple picture of CME structures as they leave the Sun [*Illing and Hundhausen*, 1985]. Filament material is normally at the back of the ICME (at the most sunward edge), separated from the sheath region by the flux rope itself. When CME1 lifted off the Sun on 20 January, remote observations by LASCO C2 showed the filament following behind the flux rope as is typical (see Figure 1).

[17] In this work, we expand on the analysis of the solar source(s) and magnetic cloud structures from F2007 and R2008 based on new evidence in the observed charge-state composition and on insights provided through further analysis of a 3-D MHD simulation of a fast ICME initially presented in *Manchester et al*. [2006, hereafter referred to as M2006]. For convenience in comparisons, we adopt the labels for features in the solar wind from F2007. The vertical dashed line (labeled SA) marks the arrival at Earth of the shock leading the ICME. Solar wind speeds in Figure 3a jumped abruptly from just over 500 km/s to nearly 900 km/s. The shock snowplowed solar wind material ahead of it, compressing it to achieve high densities (Figure 3b) and high temperatures (Figure 3c) in a sheath region following the shock.

[18] Figure 3d displays the north-south component of the interplanetary magnetic field (IMF) in the GSM (solar-magnetospheric) coordinate system. The compressed southward IMF in the sheath region on 21 January reached −28 nT. This value is comparable to the southward IMF that drives superstorms but, in this case, it lasted for less than 30 min so the storm reached only moderate intensity. Typical quiet time IMF values are 3–5 nT with ecliptic rather than southward orientations.

[19] At the vertical dashed line labeled SB, the density again began to climb. This discontinuity marked the arrival of the solar filament. Densities in this region exceeded 50

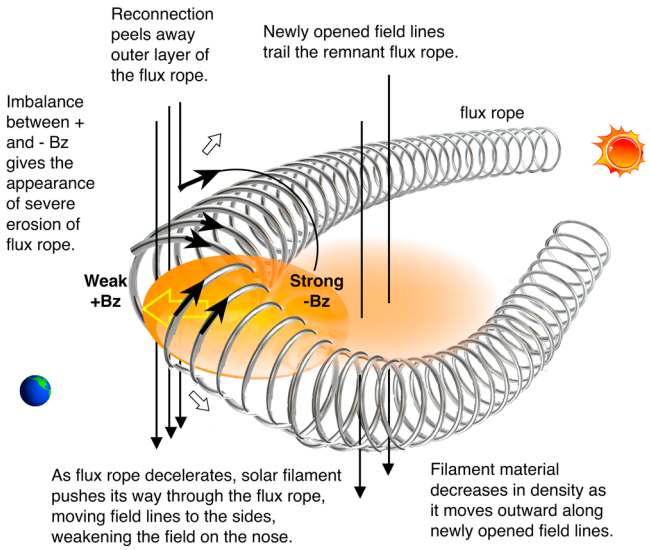

Figure 4. An illustration is given of the processes in the simulation found to be responsible for the appearance of the solar filament material directly behind the sheath region in the ICME. The solar wind flow is from right to left. Evidence that such remarkable behavior has actually occurred in the very fast CME that erupted from the Sun on 2005 January 20 (but with opposite sign of IMF *Bz*) is described in the text.

cm^{-3} and dynamic pressures reached 63 nPa if the He^{2+} component is taken into account (see F2007). Note that the temperatures in the filament (Figure 3c) were much cooler than the heated and compressed solar wind in the sheath. While the "filament" material is cooler than the sheath, it is still slightly hotter than the solar wind. Consistent with these observations, we find considerable heating of the filament material close to the Sun in the simulation of a comparable fast CME in section 3.

[20] ICMEs generally contain an enhanced ratio of He^{2+}/H^{+} and high charge states of oxygen and iron. These high charge states are thought to originate low in the solar corona or to be a product of the heating the CME undergoes during its ejection from the Sun. Cluster observed an elevated He^{2+}/H^{+} ratio in the ICME as it approached Earth's bow shock (see F2007). However, solar filaments contain a significant fraction of low charge-state ions [cf. *Wimmer-Schweingruber et al.*, 2006; *Lepri and Zurbuchen*, 2010]. While this particular ICME did not exhibit low charge states of C, O, or Fe as shown in *Lepri et al.* [2012], which only studied those elements, further examination of the SWICS data revealed the presence of a significant contribution of He^{+} within the ejecta. Similar mixtures of both low and high charge states have been seen in other He^{+}-rich events [*Gosling et al.*, 1980; *Burlaga et al.*, 1998; *Gloeckler et al.*, 1999; *Skoug et al.*, 1999]. In fact, Skoug et al. reported elevated heavy ion charge states throughout an extended interval of some of the largest He^{+}/He^{2+} values ever observed. The reasons for this blend of hot and cold material are not yet understood. *Skoug et al.* [1999] suggest two possible mechanisms: (1) partial ionization of the filament material in the solar corona which proceeds at different rates for different elements, and (2) changes in topology that mix plasmas with different frozen-in ionization states during transit to Earth.

[21] Shown in Figure 3g is the ratio of singly to doubly charged helium (He^{+}/He^{2+}) observed by the Solar Wind Ion Composition Spectrometer (SWICS) on the ACE satellite. He^{+} enters the SWICS instrument and is accelerated by a post acceleration region, where it gains ~26 keV in energy before entering the Time of Flight telescope (see *Gloeckler et al.* [1998] for more details of SWICS operation). The ion's total energy is close to the lower energy limit of detection in the instrument and therefore it remains elusive in many measurements not only because of the lack of He^{+} in the nominal solar wind but also because the energy lies near the detection threshold. He^{2+}, on the other hand, gains 2 × 26 keV (due to the 26 kV potential) in the post acceleration region and therefore is almost always above the detection limit of the solid-state detectors. The mere presence of He^{+} in this data set is rather significant and likely enabled by the very fast solar wind speeds associated with this particular CME as well as by the presence of a significant amount of filament material. The He^{+}/He^{2+} ratio (with a 2 h temporal resolution compared to the 1 min resolution in the other solar wind parameters) was enhanced in the ICME, maximizing at the peak in plasma density following the sheath. This ratio fell below instrument thresholds outside of the values shown and therefore no measurements exist before and after the solid line.

[22] It is worth noting that the sheath region, which should contain predominantly solar wind plasma swept up in front of the ICME during its transit to Earth, also contains significant low charge-state helium (Figure 3g). This is consistent with the magnetic reconnection observed by the Cluster spacecraft at 18:39:30 UT and 18:45:00 UT [*Munoz et al.*, 2010; *Chian and Munoz*, 2011, 2012] at the leading edge of the high-density region (identified here as the solar filament). These times occur on either side of the sharp northward IMF spike just before the vertical dashed line labeled SB in Figure 3. In reconnection, magnetic field lines that thread the sheath and those associated with the filament material are broken and reconnected with each other. In the process, filament material is mixed with sheath plasma. As will be described later, this reconnection, pictured at the leading edge of the flux rope in Figure 4, contributed to the observed redistribution of the filament material within the ICME.

[23] Figure 3f gives the pitch angles of suprathermal (272 eV) solar wind electrons called "strahl," which flow nearly continuously along magnetic field lines outward from the Sun (shown also in F2007). The strahl is used as an indicator of the connectivity of magnetic field lines. A single strahl component moving away from the Sun parallel to the IMF indicates an open magnetic field line connected at only one end to the Sun. However, bidirectional strahl electrons traveling both parallel (0°) and antiparallel (180°) to the IMF indicate a closed magnetic field topology still connected to the Sun at both ends [cf. *Shodhan et al.*, 2000]. As discussed in F2007, observations in Figure 3f first show an isotropic pitch angle distribution within the sheath between SA and SB due to heating of the solar wind electrons at and behind the shock. Moving into the leading edge of the filament, starting at SB, bidirectional strahl electrons are seen, indicating a closed magnetic topology. We will show in section 3 on the basis of the simulation of a comparable fast

CME that this structure is consistent with a remnant flux rope, in which azimuthal fields have been eroded by reconnection with the sheath fields and by transport of flux away from the apex of the flux rope by diverging nonradial flows. Because of the removal of flux from the leading edge, the southward IMF portion of the flux rope is very short-lived (~10 min) followed by a rotation to a much longer interval of obliquely northward IMF. The region of recently opened field lines trailing the remnant flux rope (which closer to the Sun were part of the more extended magnetic cloud structure) is marked by a change to more purely northward IMF at 21:40 UT. The transition from obliquely to more purely northward IMF can be clearly seen in the IMF clock angles plotted in Figure 3e. A 0° clock angle indicates due northward IMF, ±90° indicates horizontal IMF in the ecliptic plane, and ±180° indicates due southward IMF. The region of the remnant flux rope (region 2) in Figure 3 has an obliquely northward IMF clock angle containing a significant or dominant IMF *By* component. The clock angle changes abruptly to due northward in the region of opened field lines trailing the remnant flux rope (labeled region 3 in the figure). This transition is accompanied by an abrupt weakening in the sunward directed strahl component.

[24] *Ruffenach et al*. [2012] conducted a study of a magnetic cloud being eroded by reconnection that was observed by STEREO A, STEREO B, ACE, Wind, and THEMIS. They found that the strahl contained information on the connection to the Sun. A significant complication is that the exact topology produced in this process and its connectivity to the Sun (both of which are unknown) are critical for understanding the changes in the strahl distribution. However, the very existence of abrupt changes in the strahl closely associated with the remnant flux rope and trailing opened field lines provide supporting evidence for the existence of the topological changes required by this interpretation of the solar wind and IMF observations. Another abrupt change in the strahl early on 22 January signaled the arrival of southward fields in the second MCL structure identified by F2007.

3. The Connection to the Sun

[25] We will return later to a discussion of the geospace response summarized in Figures 3h–3k but first we explore the source of the high-density plasma in the ICME and the mechanisms that moved it behind the sheath region. To do this, we compare the observations of the 21 January CME with a simulation of another very fast CME described in M2006 with lift-off speeds of 4000 km/s dropping to 2000 km/s by 1 AU in which dense plasma also appeared directly following the sheath. The details of the model and the initial conditions for the simulation are described therein. By following the simulation backward in time after the dense plasma appears behind the sheath region, we are able in the present study to trace its origins unambiguously to the erupting filament and examine the mechanisms that resulted in the redistribution of the filament material.

[26] Figure 4 illustrates the changes in the magnetic cloud and solar filament during propagation to Earth as seen in the simulation. The solar wind flow is from right to left in the figure. There are two factors strongly affecting the topology of the flux rope as it travels to Earth. As the CME

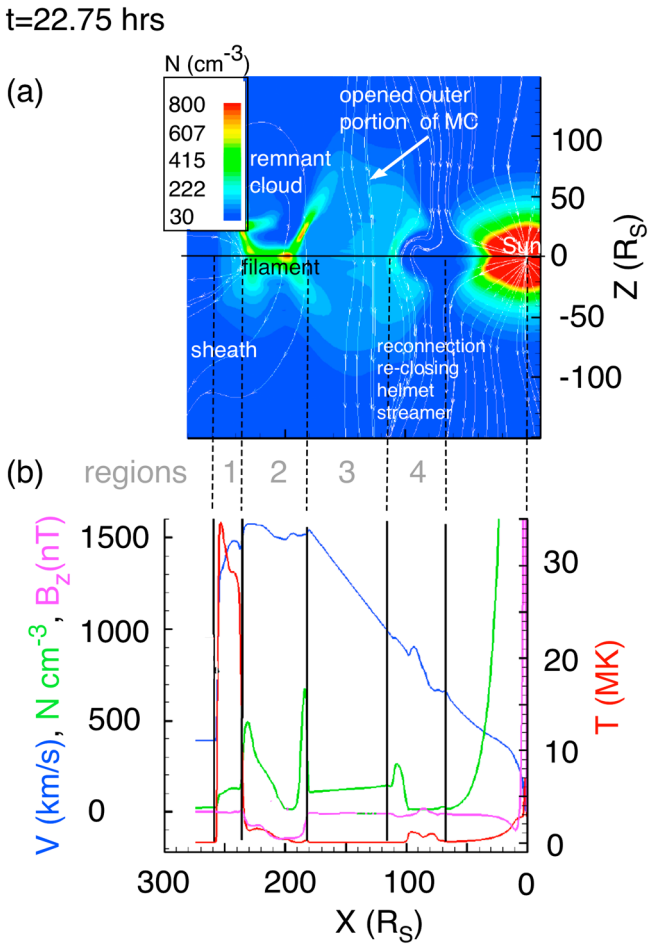

Figure 5. (a) A cross section of solar wind density in the *XZ* plane showing the sheath (region 1), remnant flux rope (region 2), opened outer flux rope (region 3), and continuing reconnection region near the Sun that recloses the helmet streamer (region 4). (b) Line extractions of solar wind parameters are taken along $Z = 0$. Shown are the velocity (blue), density (green), temperature (red), and IMF *Bz* (purple). All of the main features in regions 1–3 also appear in the observations on 21 January 2005 (Figure 3) but with opposite sign of IMF *Bz*.

slows, the momentum of the solar filament material forces it to move through the flux rope, diverting magnetic flux around to the sides with an associated weakening of the magnetic field at the nose. As a result, the northward IMF at the leading edge of the flux rope is weaker than the southward IMF at the back. This imbalance creates the impression of a flux rope severely eroded by reconnection at its leading edge.

[27] In addition to this distortion of the flux rope by the solar filament, reconnection is also occurring between the closed field lines at the leading edge of the flux rope and the IMF in the sheath region. In the case of the 21 January 2005 flux rope, this reconnection is confirmed by Cluster observations [*Munoz et al*., 2010; *Chian and Munoz*, 2011, 2012]. The reconnection in the simulation and observations opens up the initially larger magnetic flux rope structure peeling away its outer layers. In their analysis of another magnetic cloud undergoing reconnection at its leading edge

but without solar filament material, *Dasso et al*. [2006, 2007] find that magnetic flux is removed from the front of the remnant flux rope but not from behind. The opened field lines trailing the remnant flux rope easily turned northward and straightened as they were peeled away. However, the IMF *By* component in the remnant flux rope must strengthen to maintain pressure balance in the magnetic cloud structure. The differential velocity from the front to the back of the strongly expanding magnetic cloud structure results in a spreading of magnetic field lines in the trailing portion of the ICME and a weakening of the magnetic field strength. These effects lead to a magnetic cloud structure that is asymmetric in both the strength and rotation of the magnetic field. The present study adds the response of the filament material as a new feature to the evolution of the eroding flux rope discussed by *Dasso et al*. [2006, 2007]. Filament material on recently opened field lines spreads outward to fill the associated larger volume of space and filament densities decrease everywhere except inside the remnant flux rope itself.

[28] For ease of comparison to solar wind features in the 21 January 2005 event, we present line extractions in Figure 5b of simulated solar wind velocity, density, temperature, and IMF *Bz* along the Sun-Earth line at an elapsed time of 22.75 h as the flux rope approaches the Earth. Figure 5a gives a cross section of solar wind density in the *XZ* plane for global context. Line extractions of solar wind parameters are taken along the $Z = 0$ line. The sheath (region 1), remnant flux rope (region 2), opened outer flux rope (region 3), and continuing reconnection region near the Sun that recloses the helmet streamer (region 4) are delineated by the vertical dashed lines. The key features in the density are the presence of filament material directly behind the sheath, the narrow peak in density at the back of the remnant flux rope, and the lower filament densities on the recently opened field lines trailing behind. Key features in the temperatures (red) are the hot sheath material followed by the much cooler dense filament. The azimuthal (*Bz*) flux (purple) is entirely unbalanced giving the appearance of a flux rope severely eroded by reconnection on the front side. There is essentially no +*Bz* component in the ICME fields. Key features in the velocity are the rise in velocity from the sheath moving into the flux rope, the relatively constant velocity in the flux rope, and the decreasing velocities in the trailing region of recently opened field lines. All of these features also appear in the observations on 21 January 2005 (see Figure 3) but with opposite sign in the IMF *Bz*. A reconnection jet develops near the Sun as the helmet streamer reforms. The reconnection jet creates a dimple in the density at the trailing edge of the ICME. The signatures of reconnection are the velocity and density enhancements on the sunward side of the filament seen in line extractions in Figure 5b. A counterpart of this region is not seen in the 21 January 2005 observations.

[29] We calculate the rate of reconnection in the simulation and find that the CME retains 93% of its flux despite reconnection with the IMF during transport to 1 AU. The transport of the flux away from the apex of the flux rope in this case is considerably more important than reconnection with the IMF.

[30] We find evidence for the processes described in the simulation in observations of the fast ICME on 21 January 2005, however, with opposite sign of the IMF *Bz*. In Figure 3, corresponding regions 1–3 are labeled. Consistent with the simulation, the observed IMF *Bz* cutting through the flux rope was entirely unbalanced. A very short interval of strong southward IMF at the leading edge of the flux rope was followed by a much longer interval of weaker obliquely northward IMF. Counterstreaming strahl electrons indicate this region was still connected at both ends to the Sun. The observed peak in the filament density was located directly behind the ICME sheath region. The reconnection at the nose of the ICME was observed by the Cluster spacecraft [*Munoz et al*., 2010]. This is consistent with the remnant flux rope labeled region 2 in the simulation. An abrupt transition to more purely northward IMF coincident with a decrease in the sunward strahl is consistent with the region of newly open field lines in the simulation trailing the remnant flux rope (labeled region 3). In both the simulation and the observations, the filament density drops in this region as the filament material moves outward along opened field lines. The remarkable similarities between the modeled fast ICME and the 21 January event, described above, provide strong evidence that the same mechanisms were at work in each. The erosion of southward IMF from the front of the ICME very likely protected the Earth from a much more severe geomagnetic storm.

[31] The close correspondence between features in the simulation at the center of the flux rope and in the observations on 21 January at greater than 60° from the longitude of the eruption, which was at 14°N, 67°W, is surprising. However, 3-D reconstructions of the density structure of the 21 January 2005 CME by the Solar Mass Ejection Imager (SMEI) clearly indicate that the CME had a large longitudinal extent spanning 90° [*Jackson et al*., 2009]. The tomography shows two dense lobes, one at the longitude of the originating active region and one that directly passed the Earth. Furthermore, there is a dense driver behind the shock seen in the SMEI 3-D reconstructions, which is not inconsistent with the dense filament material observed at 1 AU.

[32] Figure 6 presents snapshots of the density (Figure 6a) and the entropy (Figure 6b) of the plasmas in the simulated ICME. Color contours of density are shown in the $Y = 0$ plane behind the 3-D flux rope. Color contours of nonradial plasma flow are given in the $Z = 0$ plane below the flux rope. The Sun is to the far right and the Earth is beyond the left edge of the figure. The white lines are magnetic field lines newly opened by reconnection at the leading edge of the flux rope that straighten as they peel away and trail behind the remnant flux rope. This trailing region is labeled as region 3 in Figures 3 and 5. The red lines are the remaining closed field lines of the remnant flux rope (labeled as region 2 in Figures 3 and 5). The high density (red) of the solar filament is seen within the remnant flux rope, decreasing to lower values (yellow to green) moving into the region of opened field lines trailing behind. The high densities (red) to the far right are in the vicinity of the Sun, itself. Much lower densities (light blue) are seen in the sheath region preceding the flux rope (labeled as region 1 in Figures 3 and 5). In the $Z = 0$ plane, diverging nonradial flows (blue) at the nose of the flux rope move magnetic field lines to the sides as the filament pushes forward toward the sheath region.

[33] In Figure 6b, entropy values are plotted in the $Y = 0$ plane behind the 3-D flux rope and the magnitude of IMF *Bz* is shown in the $Z = 0$ plane below. The shocked and heated solar wind plasma in the sheath region upstream of the flux

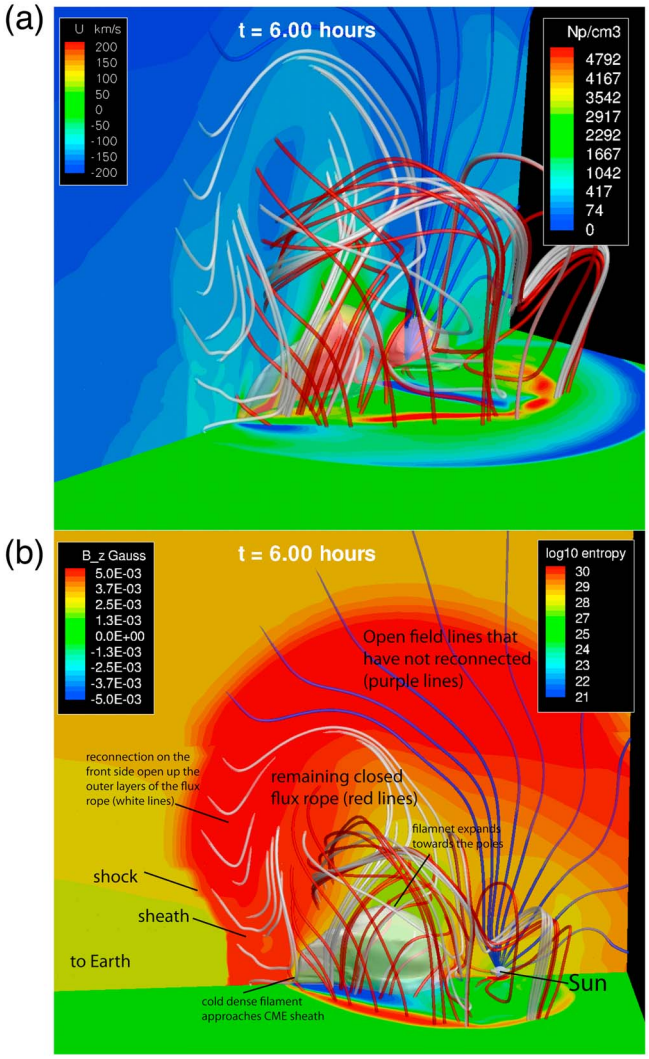

Figure 6. The flux rope interaction is shown with the ambient solar wind in the simulation. The 3-D structure of the ICME appears. Reconnecting field lines at the front of the flux rope that are straightening out and trailing behind are shown in white. The remaining closed field lines of the remnant flux rope are shown in red. (a) The log density is plotted in the $Y=0$ plane behind the flux rope and the nonradial flows in the $Z=0$ plane below the flux rope. (b) The entropy is plotted in the $Y=0$ plane and the IMF *Bz* in the $Z=0$ plane. See text for details.

rope has high entropy values (orange-red) while the cool, dense plasma of the solar filament has low entropy values (green). Though not shown here, the simulation indicates that although the filament material is still cooler than the sheath plasma, it has undergone considerable heating shortly after initiation. Its temperature is slightly cooler than the background solar wind. At the nose of the flux rope, cold dense plasma is seen approaching the CME sheath region. Nonradial flows at the nose in Figure 6a move magnetic flux to the sides of the solar filament creating a "bald spot" in the flux rope (seen as a thinning of the IMF *Bz* contours in the $Z=0$ plane in Figure 6b). Both reconnection and the diversion of magnetic flux to the sides of the filament erode the magnetic flux at the nose of the flux rope.

[34] The density of the solar filament within the ICME on 21 January was extreme. Typical ICMEs have densities that are comparable to the solar wind in which they are embedded [*Crooker et al.*, 2000]. The highest densities are typically associated with the shocked and compressed solar wind in the sheath region ahead of them. The 21 January 2005 ICME represents a significant departure from the typical solar wind driving during magnetic storms.

4. The One-Two Punch of the Solar Filament

[35] Returning to Figures 3h–3k, we examine geospace observations showing the response to the solar filament impact. Figure 3h displays *SYM-H*, a high-time-resolution index describing the magnetic field depression at the Earth's surface during a magnetic storm [*Iyemori*, 1990]. It is similar to *Dst* but with a resolution of 1 min compared to 1 h for *Dst* [*Wanliss and Showalter*, 2006]. Though the ring current is thought to make the largest contribution to *SYM-H* [*Kozyra and Liemohn*, 2003], there are also contributions from magnetic fields generated by magnetopause, field-aligned and magnetotail currents, as well as induced currents in the solid Earth [cf. *Carovillano and Siscoe*, 1973; *McPherron*, 1997; *Liemohn and Kozyra*, 2003]. The *SYM-H** curve is the observed *SYM-H* with these additional contributions removed [*Burton et al.*, 1975; *Langel and Estes*, 1985]. In this form, *SYM-H** is directly proportional to the total energy of the ions that comprise the storm time ring current [*Dessler and Parker*, 1959; *Sckopke*, 1966; *Liemohn*, 2003]. Because of this, it also serves as a convenient measure of the severity of the magnetic storm.

[36] Minimum *SYM-H** values around −100 nT (seen here) identify an intense magnetic storm [*Gonzalez et al.*, 1994]. When the IMF turns northward, *SYM-H** values normally recover toward a quiet time baseline as the ring current ions cease to be replenished by drifts earthward from the magnetotail and are removed by collisions and loss at the dayside magnetopause. Surprisingly, the ring current in the 21 January 2005 magnetic storm continued to grow (*SYM-H** to decrease) for three more hours after the IMF turned northward. This highly unusual development of *Dst* was first reported by *Du et al.* [2008].

[37] During northward IMF, a newly recognized mode of interaction has been found between the solar wind and Earth's magnetosphere in which large amounts of solar wind plasma can be captured by the magnetosphere [cf. *Palmroth et al.*, 2006; *Li et al.*, 2008]. In this mode, reconnection occurs between IMF and magnetospheric field lines at locations poleward of the cusps. Interplanetary magnetic flux tubes filled with filament material become magnetospheric flux tubes capturing the filament material directly into the magnetosphere. This means that helium-rich solar filament material filled the magnetosphere, creating a cold dense plasma sheet that flowed into and through the inner magnetosphere as the solar filament passed by Earth.

[38] Figure 3j gives nightside plasma sheet densities observed by the Magnetospheric Plasma Analyzer (MPA) instrument on the Los Alamos National Laboratory geosynchronous satellites [*Bame et al.*, 1993; *Thomsen et al.*, 1997]. Densities in this region are normally 0.5–2 cm^{-3} [*Borovsky et al.*, 1997], but 1 h after the arrival of the solar filament material, the plasma sheet densities increased to

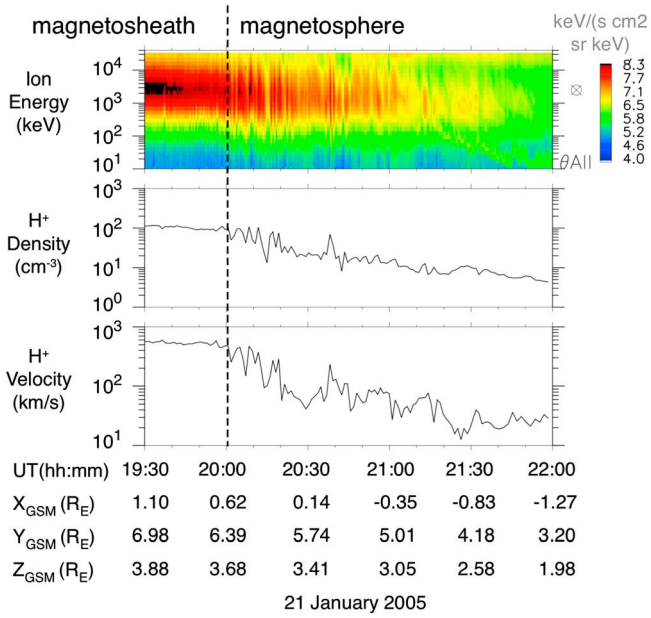

Figure 7. The Double Star TC-1 satellite observed the entry of the solar filament material during northward IMF conditions as it crossed from the magnetosheath into the magnetosphere near local noon. (top) Ions at typical magnetosheath energy and density are seen within the magnetosphere. (middle) The drop in density from magnetosheath values near 100 cm^{-3} to values more typical of a cold dense plasma sheet 5–10 cm^{-3} is shown as TC-1 moves from the magnetosheath through the low-latitude boundary layer and into the inner magnetosphere. (bottom) The vertical dashed line marks the transition in ion speeds from magnetosheath to magnetospheric values.

extreme values of up to 6 cm^{-3}. These are typical of cold dense plasma sheets [*Lavraud et al.*, 2005, 2006] which have densities > 2 cm^{-3} and temperatures < 5 keV at geosynchronous orbit. The Double Star TC-1 satellite [*Liu et al.*, 2005; *Reme et al.*, 2005] crossing from the magnetosheath into the magnetosphere between 20 UT and 22 UT directly observed the entry of the solar filament material (see Figure 7).

[39] Strong magnetotail stretching is not expected under conditions associated with northward IMF and yet strong stretching is seen in the b2i index (Figure 3i). The b2i index at 20–24 magnetic local time gives the location in magnetic latitude of the transition between dipolar and stretched magnetic field lines [*Newell et al.*, 1998]. The lower the magnetic latitude of the b2i, the more stretched is the magnetotail. As the magnetotail stretching reached its maximum value (minimum magnetic latitude), the geosynchronous satellites on the nightside entered the magnetotail lobes, indicated by the dropout in geosynchronous density. When the stretching diminished somewhat, the satellites reentered the plasma sheet to observe a cooler but still superdense plasma sheet. The magnetic field stretching during northward IMF is due to the development of a plasma sheet that despite its cold temperatures is so dense as to be able to alter the topology of the magnetotail through diamagnetic effects. Since cold dense plasma sheets are typically found after extended intervals of northward IMF (and quieting magnetic activity), they have so far not been associated with significant magnetotail stretching. In contrast, during southward IMF, the plasma sheet has much lower density but is hotter so that plasma pressures and pressure gradients routinely produce significant changes in the large-scale topology of the magnetotail. How frequently plasmas during northward IMF become dense enough to produce the strong magnetotail stretching seen in this event and the consequences throughout geospace are open questions, but a condition of strong stretching during northward IMF, as seen in this event, has not been previously reported.

[40] Figure 3k presents the *AU* and *AL* indices [*Davis and Sugiura*, 1966] produced by the World Data Center in Kyoto, Japan. These indices are representative of the level of convection and magnetic activity, respectively, in the auroral oval [*Kamide and Akasofu*, 1983; *Kamide and Rostoker*, 2004]. Surprisingly enough, magnetic activity levels in the auroral region indicated by the *AL* index were low at the time of maximum magnetotail stretching. The rise in the *AU* index indicates that convection was enhanced as the solar filament compressed the magnetosphere bringing the cold dense plasma sheet earthward. During this interval the magnetic storm reached its peak (indicated by the minimum in *SYM-H** in Figure 3h).

5. Summary and Implications

[41] To summarize, a continuing mystery surrounds the fate of dense solar filament material that is expelled from the Sun into interplanetary space during coronal mass ejections. Though solar filaments are frequently observed moving outward from the Sun in CMEs, they seldom are recognizable in ICMEs that arrive at Earth. The conditions under which filaments reach Earth are of great interest because dense solar wind intensifies the damaging effects of geomagnetic storms. On 21 January 2005, an interplanetary CME containing solar filament material hit the Earth's magnetosphere offering a rare opportunity to investigate the processes that enable the transport of filaments to Earth and their space weather consequences. The filament material was identified based on an elevated He^{+}/He^{2+} ratio. We show by comparison between solar wind observations at 1 AU and a simulation of a fast CME that three unusual processes combined to move the filament directly behind the sheath, a configuration different from that observed near the Sun. In the simulation, as the ICME decelerates moving toward Earth, the momentum of the dense filament material, originally at the back (sunward edge) of the flux rope, causes it to push its way forward toward the nose. A portion of the filament material pushes so far forward that it comes into direct contact with the sheath material surrounding the ICME. Diverging nonradial flows develop around the filament, which transport azimuthal flux from in front to the sides of the ICME. At the same time, magnetic field lines at the nose of the ICME reconnect with the IMF, peeling away the outer layer and creating a region of opened field lines trailing behind. However, during the short propagation time, only 7% of the azimuthal magnetic flux is lost by reconnection, so the vast majority of the flux imbalance in front of the filament is due to divergent flows. This transport process offers an additional mechanism to explain flux rope erosion, which is particularly applicable to fast CMEs. Observations show evidence that these processes occurred

during the 21 January ICME. Within 1 h after impact on the magnetosphere, a superdense plasma sheet formed from the solar filament material and continued to move high-density material through the magnetosphere for the entire ~6 h of the filament passage. Observations indicate that strong magnetotail stretching due to diamagnetic effects accompanied the cold dense plasma sheet despite the northward IMF conditions and weak levels of magnetic activity at this time.

[42] These conditions were linked to an array of anomalous and extreme features in the magnetosphere and ionosphere, including a brief equatorial superfountain and strong ion-atom aurora. Until now, both have been observed almost exclusively during superstorms [cf. *Basu et al*., 2001; *Tsurutani et al*., 2004; *Zhang et al*., 2006b] Moreover, during the passage of the filament, high-energy ion precipitation peaked in intensity, a significant oxygen component of the ring current developed in the inner magnetosphere, the equatorward edge of the diffuse aurora remained at midlatitudes for more than 6 h, and the equatorial ionization anomaly crests intensified. These features were highly unusual because they appeared during northward IMF conditions which are normally associated with magnetic quieting. The reasons why significant solar filament material made it to Earth in this case and not others and the connections between the solar filament and these geospace features will be examined in follow-on papers.

[43] The analysis here demonstrates the potential for a significant solar filament collision to amplify the effects of an ICME on the Earth's space environment through the rapid formation of cold dense plasma sheets in a compressed magnetosphere. But the implications are far-reaching. If the IMF had rotated southward after the formation of the superdense plasma sheets, the dense material would have been transported earthward providing the source population for an extreme ring current and triggering a superstorm [cf. *Zhang et al*., 2006a; *Liemohn et al*., 2008]. This two-stage capture and energization process has been observed in more moderate events [*Thomsen et al*., 2003] in the presence of typical high-density solar wind.

[44] Both the reconnection rate at the leading edge [cf. *Taubenschuss et al*., 2010] and the momentum of the filament material increase with the speed of the ICME. This implies that the extent of the redistribution of the filament material within the ICME and the flux rope erosion should both be a function of its speed. Recent ICMEs with significant filament material occurred in January 2005 (this event), May 1998 [*Skoug et al*., 1999], and January 1997 [*Burlaga et al*., 1998] with speeds of ~900 km/s, ~600 km/s, and ~450 km/s, respectively. Consistent with this scenario, the January 2005 event had filament material in the front of the flux rope, the May 1998 event in the center of the flux rope, and the January 1997 event at the back of the flux rope. For these very few cases where significant filament material was observed, this simple picture seems to hold but analysis of more events is required for definite conclusions to be drawn from this.

[45] Intriguing indirect evidence suggests that a similar event to January 2005, albeit under different IMF conditions and with denser solar filament material, may have occurred during the Carrington 1859 magnetic storm [*Li et al*., 2006; M2006], the largest in recorded history [cf. *Tsurutani et al*., 2003]. Unusually dense solar wind was also observed just behind the sheath during the 4–5 August 1972 event [*Vaisberg and Zastenker*, 1976; *d'Uston et al*., 1977], which disrupted a major communications system in the United States [*Boteler and van Beek*, 1999]. The August 1972 ICME is believed to be the fastest ever observed at 1 AU [*Cliver et al*., 1990]. The factors that must line up just right to intensify a major storm into a "100 year" storm are unknown. Though rare, the prediction of these extreme events is of intense interest because disastrous economic and societal impacts are anticipated should one occur in modern times [*National Research Council*, 2008].

[46] **Acknowledgments.** The authors would like to acknowledge support for the research under NASA (NNX10AQ34C, NNH09AK621, NNH11AR241, and NNX07AT186) and NSF (ATM-0903596) grants. This work was partially supported by the University of Michigan. Portions of this research were performed at the Jet Propulsion Laboratory, California Institute of Technology, under contract with NASA. Thanks to Ruth Skoug and Heather Elliott for providing reprocessed ACE solar wind parameters.

[47] Philippa Browning thanks Noe Lugaz and an anonymous reviewer for their assistance in evaluating this paper.

References

Bame, S. J., D. J. McComas, M. F. Thomsen, B. L. Barraclough, R. C. Elphic, J. P. Glore, J. T. Gosling, J. C. Chavez, E. P. Evans, and F. J. Wymer (1993), Magnetospheric plasma analyzer for spacecraft with constrained resources, *Rev. Sci. Instrum.*, *64*, 1026–1033.

Basu, S., S. Basu, K. M. Groves, H. C. Yeh, S.-Y. Su, F. J. Rich, P. J. Sultan, and M. J. Keskinen (2001), Response of the equatorial ionosphere in the South Atlantic region to the great magnetic storm of July 15, 2000, *Geophys. Res. Lett.*, *28*(18), 3577–3580.

Borovsky, J. E., M. F. Thomsen, and D. J. McComas (1997), The superdense plasma sheet: Plasmaspheric origin, solar wind origin, or ionospheric origin?, *J. Geophys. Res.*, *102*(A10), 22,089–22,097.

Boteler, D. H., and G. J. van Beek (1999), August 4, 1972 revisited: A new look at the geomagnetic disturbance that caused the L4 cable system outage, *Geophys. Res. Lett.*, *26*(5), 577–580.

Burlaga, L. F., W. H. Mish, and Y. C. Whang (1990), Coalescence of recurrent streams of different sizes and amplitudes, *J. Geophys. Res.*, *95*(A3), 4247–4255.

Burlaga, L., et al. (1998), A magnetic cloud containing prominence material: January 1997, *J. Geophys. Res.*, *103*(A1), 277–285.

Burton, R. K., R. L. McPherron, and C. T. Russell (1975), An empirical relationship between interplanetary conditions and *Dst*, *J. Geophys. Res.*, *80*(31), 4204–4214.

Carovillano, R. L., and G. L. Siscoe (1973), Energy and momentum theorems in magnetospheric processes, *Rev. Geophys.*, *11*(2), 289–353.

Chian, A. C.-L., and P. R. Munoz (2011), Detection of current sheets and magnetic reconnections at the turbulent leading edge of an interplanetary coronal mass ejection, *Astrophys. J. Lett.*, *733*(L34), doi:10.1088/2041-8205/733/2/L34.

Chian, A. C.-L., and P. R. Munoz (2012), Observation of magnetic reconnection at the turbulent leading edge of an interplanetary coronal mass ejection, in *Understanding Solar Activity: Advances and Challenges*, EAS Publications Series, vol. *55*, edited by M. Faurobert, C. Fang, and T. Corbard, pp. 327–334, Cambridge Univ. Press, New York.

Cliver, E. W., J. Feynman, and H. B. Garrett (1990), An estimate of the maximum speed of the solar wind, 1938–1989, *J. Geophys. Res.*, *95*(A10), 17,103–17,112.

Crooker, N. U., and T. S. Horbury (2006), Solar imprint on ICMEs, their magnetic connectivity, and heliospheric evolution, *Space Sci. Rev.*, *123*, 93–109, doi:10.1007/s11214-006-9014-0.

Crooker, N., S. Shodhah, J. T. Gosling, J. Simmerer, J. T. Steinberg, and S. W. Kahler (2000), Density extremes in the solar wind, *Geophys. Res. Lett.*, *27*(23), 3769–3772.

Dasso, S., C. H. Mandrini, P. Démoulin, and M. L. Luoni (2006), A new model-independent method to compute magnetic helicity in magnetic clouds, *Astron. Astrophys.*, *455*, 349–359.

Dasso, S., M. S. Nakwacki, P. Demoulin, and C. H. Mandrini (2007), Progressive transformation of a flux rope to an ICME: Comparative analysis using the direct and fitted expansion methods, *Sol. Phys.*, *244*, 115–137.

Davis, T. N., and M. Sugiura (1966), Auroral electrojet activity index *AE* and its universal time variations, *J. Geophys. Res.*, *71*(3), 785–801.

Dessler, A. J., and E. N. Parker (1959), Hydromagnetic theory of magnetic storms, *J. Geophys. Res.*, *64*(12), 2239–2252.

Du, A. M., B. T. Tsurutani, and W. Sun (2008), Anomalous geomagnetic storm of 21–22 January 2005: A storm main phase during northward IMFs, *J. Geophys. Res.*, *113*, A10214, doi:10.1029/2008JA013284.

D'Uston, C., J. M. Bosqued, F. Cambou, V. V. Temnyi, G. N. Zastenker, O. L. Vaisberg, and E. G. Eroshenko (1977), Energetic properties of interplanetary plasma at the Earth's orbit following the August 4, 1972 flare, *Sol. Phys.*, *51*, 217–229.

Farrugia, C. J., et al. (2002), Wind and ACE observations during the great flow of 1–4 May 1998: Relation to solar activity and implications for the magnetosphere, *J. Geophys. Res.*, *107*(A9), 1240, doi:10.1029/2001JA000188.

Farrugia, C. J., V. K. Jordanova, M. F. Thomsen, G. Lu, S. W. H. Cowley, and K. W. Ogilvie (2006), A two-ejecta event associated with a two-step geomagnetic storm, *J. Geophys. Res.*, *111*, A11104, doi:10.1029/2006JA011893.

Forsyth, R. J., et al. (2006), ICMEs in the inner heliosphere: Origin, evolution, and propagation effects. Report of Working Group G, *Space Sci. Rev.*, *123*, 383–416, doi:10.1007/s11214-006-9022-0.

Foullon, C., C. J. Owen, S. Dasso, L. M. Green, I. Dandouras, H. A. Elliott, A. N. Fazakerley, Y. V. Bogdanova, and N. U. Crooker (2007), Multi-spacecraft study of the 21 January 2005 ICME: Evidence of current sheet substructure near the periphery of a strongly expanding fast magnetic cloud, *Sol. Phys*, *244*, 139–165.

Gilbert, J. A., S. T. Lepri, E. Landi, and T. H. Zurbuchen (2012), First measurements of the complete heavy-ion charge state distributions of C, O, and Fe associated with interplanetary coronal mass ejections, *Astrophys. J.*, *751*, 20, doi:10.1088/0004-637X/751/1/20.

Gloeckler, G., et al. (1998), Investigation of the composition of solar and interstellar matter using solar wind and pickup ion measurements with SWICS and SWIMS on the ACE spacecraft, *Space Sci. Rev.*, *86*, 497–539.

Gloeckler, G., L. A. Fisk, S. Hefti, N. A. Schwadron, T. H. Zurbuchen, F. M. Ipavich, J. Geiss, P. Bochsler, and R. F. Wimmer-Schweingruber (1999), Unusual composition of the solar wind in the 2–3 May 1998 CME observed with SWICS on ACE, *Geophys. Res. Lett.*, *26*(2), 157–160.

Gonzalez, W. D., J. A. Joselyn, Y. Kamide, H. W. Kroehl, G. Rostoker, B. T. Tsurutani, and V. M. Vasyliunas (1994), What is a geomagnetic storm?, *J. Geophys. Res.*, *99*(A4), 5771–5792.

Gopalswamy, N., M. Shimojo, W. Lu, S. Yashiro, K. Shibasaki, and R. A. Howard (2003), Prominence eruptions and coronal mass ejection: A statistical study using microwave observations, *Astrophys. J.*, *586*(1), 562–578.

Gosling, J. T., J. R. Asbridge, S. J. Bame, W. C. Feldman, and R. D. Zwickl (1980), Observations of large fluxes of He^{+} in the solar wind following an interplanetary shock, *J. Geophys. Res.*, *85*(A7), 3431–3434.

Gruesbeck, J. R., S. T. Lepri, and T. H. Zurbuchen (2012), Two Plasma Model for low charge state ICME Observations, *Astrophys. J.*, *760*, 141.

Illing, R. M. E., and A. J. Hundhausen (1985), Observation of a coronal transient from 1.2 to 6 Solar radii, *J. Geophys. Res.*, *90*(A1), 275–282.

Iyemori, T. (1990), Storm-time magnetospheric currents inferred from mid-latitude geomagnetic field variations, *J. Geomagn. Geoelectr.*, *42*, 1249–1265.

Jackson, B. V., P. P. Hick, A. Buffington, M. M. Bisi, J. M. Clover, M. S. Hamilton, M. Tokumaru, and K. Fujiki (2009), 3D-reconstruction of density enhancements behind interplanetary shocks from the Solar Mass Ejection Imager white-light observations, CP1216, *Twelfth International Solar Wind Conference*, edited by M. Maksimovic, K. Issautier, N. Meyer-Vernet, M. Moneuquet, and F. Pantellini, pp. 659–662, American Institute of Physics, Melville, N.Y.

Kamide, Y., and S.-I. Akasofu (1983), Notes on the auroral electrojet indices, *Rev. Geophys.*, *21*(7), 1647–1656.

Kamide, Y., and G. Rostoker (2004), What is the physical meaning of the *AE* index?, *Eos Trans. AGU*, *85*(19), 188–192.

Kozyra, J. U., and M. W. Liemohn (2003), Ring current energy input and decay, *Space Sci. Rev.*, *109*, 105–131.

Langel, R. A., and R. H. Estes (1985), Large-scale, near-field magnetic fields from external sources and the corresponding induced internal field, *J. Geophys. Res.*, *90*(B3), 2487–2494.

Laundal, K. M., and N. Østgaard (2008), Persistent global proton aurora caused by high solar wind dynamic pressure, *J. Geophys. Res.*, *113*, A08231, doi:10.1029/2008JA013147.

Lavraud, B., M. H. Denton, M. F. Thomsen, J. E. Borovsky, and R. H. W. Friedel (2005), Superposed epoch analysis of dense plasma access to geosynchronous orbit, *Ann. Geophys.*, *23*, 2519–2529.

Lavraud, B., M. F. Thomsen, S. Wing, M. Fujimoto, M. H. Denton, J. E. Borovsky, A. Aasnes, K. Seki, and J. M. Weygand (2006), Observation of two distinct cold, dense ion populations at geosynchronous orbit: Local time asymmetry, solar wind dependence and origin, *Ann. Geophys.*, *24*, 3451–3465.

Lepping, R. P., D. B. Berdichevsky, A. Szabo, C. Arqueros, and A. J. Lazarus (2003), Profile of an average magnetic cloud at 1 AU for the quiet solar phase: Wind observations, *Sol. Phys.*, *212*, 425–444.

Lepri, S. T., and T. H. Zurbuchen (2010), Direct observational evidence of filament material within interplanetary coronal mass ejections, *Astrophys. J. Lett.*, *723*, L22–L27.

Lepri, S. T., J. M. Laming, C. E. Rakowski, and R. von Steiger (2012), Spatially dependent heating and ionization in an ICME observed by both ACE and Ulysses, *Astrophys. J.*, *760*, 105–15, doi:10.1088/0004-637X/760/2/105.

Li, W., J. Raeder, M. F. Thomsen, and B. Lavraud (2008), Solar wind plasma entry into the magnetosphere under northward IMF conditions, *J. Geophys. Res.*, *113*, A04204, doi:10.1029/2007JA012604.

Li, X., M. Temerin, B. T. Tsurutani, and S. Alex (2006), Modeling of 1–2 September 1859 super magnetic storm, *Adv. Space Res.*, *38*, 273–279.

Liemohn, M. W. (2003), Yet another caveat to the Dessler-Parker-Sckopke relation, *J. Geophys. Res.*, *108*(A6), 1251, doi:10.1029/2003JA009839.

Liemohn, M. W., and J. U. Kozyra (2003), Lognormal form of the ring current energy content, *J. Atmos. Sol. Terr. Phys.*, *65*, 871–886.

Liemohn, M. W., J.-C. Zhang, M. F. Thomsen, J. E. Borovsky, J. U. Kozyra, and R. Ilie (2008), Superstorms at geosynchronous orbit: How different are they?, *Geophys. Res. Lett.*, *35*, L06S06, doi:10.1029/2007GL031717.

Liou, K., P. T. Newell, J. Shue, C. Meng, Y. Miyashita, H. Kojima, and H. Matsumoto (2007), "Compression aurora": Particle precipitation driven by long-duration high solar wind ram pressure, *J. Geophys. Res.*, *112*, A11216, doi:10.1029/2007JA012443.

Liu, Z. X., C. P. Escoubet, Z. Pu, H. Laakso, J. K. Shi, C. Shen, and M. Hapgood (2005), The Double Star mission, *Ann. Geophys.*, *23*, 2707–2712.

Lugaz, N., W. B. Manchester IV, and T. I. Gombosi (2005), Numerical simulation of the interaction of two coronal mass ejections from Sun to Earth, *Astrophys. J.*, *634*, 651–662, doi:10.1086/491782.

Lyons, L. R. (2000), Geomagnetic disturbances: Characteristics of, distinction between types, and relations to interplanetary conditions, *J. Atmos. Sol. Terr. Phys.*, *62*, 1087–1114.

Manchester, W. B., IV, A. J. Ridley, T. I. Gombosi, and D. L. Dezeeuw (2006), Modeling the Sun-to-Earth propagation of a very fast CME, *Adv. Space Res.*, *38*, 253–262.

McPherron, R. L. (1997), The role of substorms in the generation of magnetic storms, in *Magnetic Storms*, Geophys. Monogr. Ser., vol. *98*, edited by B. T. Tsurutani et al., pp. 131–148, AGU, Washington, D. C.

Munoz, P. R., et al. (2010), in Solar and stellar variability: Impact on Earth and planets, *Proceedings IAU Symposium* No. 264, edited by A. G. Kosovichev, A. H. Andrei, J.-P. Rozelot, pp. 369–372, International Astronomical Union, Paris, France.

National Research Council (2008), Severe space weather events—Understanding societal and economic impacts workshop report.

Newell, P. T., V. A. Sergeev, G. R. Bikkuzina, and S. Wing (1998), Characterizing the state of the magnetosphere: Testing the ion precipitation maxima latitude (b2i) and the ion isotropy boundary, *J. Geophys. Res.*, *103*, 4739–4745.

Palmroth, M., T. V. Laitinen, and T. I. Pulkkinen (2006), Magnetopause energy and mass transfer: Results from a global MHD simulation, *Ann. Geophys.*, *24*(A3), 3467–3480.

Pohjolainen, S., L. van Driel-Gesztelyi, J. L. Culhane, P. K. Manoharan, and H. A. Elliott (2007), CME propagation characteristics from radio observations, *Sol. Phys.*, *244*, 167–188.

Reme, H., et al. (2005), The HIA instrument on board the Tan Ce 1 Double Star near-equatorial spacecraft and its first results, *Ann. Geophys.*, *23*, 2757–2774.

Richardson, I. G., E. W. Cliver, and H. V. Cane (2001), Sources of geomagnetic storms for solar minimum and maximum conditions during 1972–2000, *Geophys. Res. Lett.*, *28*(13), 2569–2572.

Rodriguez, L., et al. (2008), Magnetic clouds seen at different locations in the heliosphere, *Ann. Geophys.*, *26*, 213–229.

Ruffenach, A., et al. (2012), Multispacecraft observation of magnetic cloud erosion by magnetic reconnection during propagation, *J. Geophys. Res.*, *117*, A09101, doi:10.1029/2012JA017624.

Rust, D. M. (1999), in *Magnetic Helicity in Space and Laboratory Plasmas*, Geophys. Monogr. Ser., vol. *111*, edited by M. R. Brown, R. C. Canfield, and A. A. Pevtsov, pp. 221–227, AGU, Washington, D.C.

Sckopke, N. (1966), A general relation between the energy of trapped particles and the disturbance field near the Earth, *J. Geophys. Res.*, *71*(13), 3125–3130.

Sharma, R., N. Srivastava, D. Chakrabarty, C. MoÅNstl, and Q. Hu (2013), Interplanetary and geomagnetic consequences of 5 January 2005 CMEs associated with eruptive filaments, *J. Geophys. Res. Space Physics*, *118*, 3954–3967, doi:10.1002/jgra.50362.

Shodhan, S., N. U. Crooker, S. W. Kahler, R. J. Fitzenreiter, D. E. Larson, R. P. Lepping, G. L. Siscoe, and J. T. Gosling (2000), Counterstreaming electrons in magnetic clouds, *J. Geophys. Res.*, *105*(A12), 27,261–27,268, doi:10.1029/2000JA000060.

Skoug, R. M., et al. (1999), A prolonged He^{+} enhancement within a coronal mass ejection in the solar wind, *Geophys. Res. Lett.*, *26*(2), 161–164.

Stone, E. C., A. M. Frandsen, R. A. Mewaldt, E. R. Christian, D. Margolies, J. F. Omes, and F. Snow (1998), The Advanced Composition Explorer, *Space Sci. Rev.*, *86*, 1–22.

Taubenschuss, U., N. V. Erkaev, H. K. Biernat, C. J. Farrugia, C. Möstl, and U. V. Amerstorfer (2010), The role of magnetic handedness in magnetic cloud propagation, *Ann. Geophys.*, *28*(5), 1075–1100, doi:10.5194/angeo-28-1075-2010.

Thomsen, M. F., E. Noveroske, J. E. Borovsky, and D. J. McComas (1997), Calculation of moments from measurements by the Los Alamos Magnetospheric Plasma Analyzer, Rep. LA-13,566-MS, Los Alamos Natl. Lab., Los Alamos, N.M.

Thomsen, M. F., J. E. Borovsky, R. M. Skoug, and C. W. Smith (2003), Delivery of cold, dense plasma sheet material into the near-Earth region, *J. Geophys. Res.*, *108*(A4), 1151, doi:10.1029/2002JA009544.

Tsurutani, B. T., and W. D. Gonzalez (1994), The causes of geomagnetic storms during solar maximum, *Eos Trans. AGU*, *75*, 49–53.

Tsurutani, B. T., W. D. Gonzalez, F. Tang, S. I. Akasofu, and E. Smith (1988), Origin of interplanetary southward magnetic fields responsible for major magnetic storms near solar maximum (1978–1979), *J. Geophys. Res.*, *93*(A8), 8519–8531.

Tsurutani, B. T., W. D. Gonzalez, G. S. Lakhina, and S. Alex (2003), The extreme magnetic storm of 1–2 September 1859, *J. Geophys. Res.*, *108*(A7), 1268, doi:10.1029/2002JA009504.

Tsurutani, B., et al. (2004), Global dayside ionospheric uplift and enhancement associated with interplanetary electric fields, *J. Geophys. Res.*, *109*, A08302, doi:10.1029/2003JA010342.

Vaisberg, O. L., and G. N. Zastenker (1976), Solar wind and magnetosheath observations at Earth during August 1972, *Space Sci. Rev.*, *19*, 687–702.

Wang, Y. M., P. Z. Ye, and S. Wang (2003), Multiple magnetic clouds: Several examples during March–April 2001, *J. Geophys. Res.*, *108*(A10), 1370, doi:10.1029/2003JA009850.

Wanliss, J. A., and K. M. Showalter (2006), High-resolution global storm index: *Dst* versus *SYM-H*, *J. Geophys. Res.*, *111*, A02202, doi:10.1029/2005JA011034.

Weigel, R. S. (2010), Solar wind density influence on geomagnetic storm intensity, *J. Geophys. Res.*, *115*, A09201, doi:10.1029/2009JA015062.

Wimmer-Schweingruber, R. F., et al. (2006), Understanding interplanetary coronal mass ejection signatures. Report of Working Group B, *Space Sci. Rev.*, *123*, 177–216.

Zhang, J.-Ch., M. W. Liemohn, M. F. Thomsen, J. U. Kozyra, M. H. Denton, and J. E. Borovsky (2006a), A statistical comparison of hot-ion properties at geosynchronous orbit during intense and moderate geomagnetic storms at solar maximum and minimum, *J. Geophys. Res.*, *111*, A07206, doi:10.1029/2005JA011559.

Zhang, Y., L. J. Paxton, J. U. Kozyra, H. Kil, and P. C. Brandt (2006b), Nightside thermospheric FUV emissions due to energetic neutral atom precipitation during magnetic superstorms, *J. Geophys. Res.*, *111*, A09307, doi:10.1029/2005JA011152.

Zhou, X.-Y., and B. T. Tsurutani (2003), Dawn and dusk auroras caused by gradual, intense solar wind ram pressure events, *J. Atmos. Sol. Terr. Phys.*, *66*, 153–160, doi:10.1016/j.jastp.2003.09.008.

Zurbuchen, T. H., and I. G. Richardson (2006), In-situ solar wind and magnetic field signatures of interplanetary coronal mass ejections, *Space Sci. Rev.*, *123*, 31–43, doi:10.1007/s11214-006-9010-4.